

Non-equilibrium electronic transport in a one-dimensional Mott insulator

F. Heidrich-Meisner,¹ I. González,² K. A. Al-Hassanieh,³ A. E. Feiguin,⁴ M. J. Rozenberg,^{5,6} and E. Dagotto⁷

¹*Physics Department, Arnold Sommerfeld Center for Theoretical Physics, and Center for NanoScience, Ludwig-Maximilians-Universität München, D-80333 München, Germany**

²*Centro de Supercomputación de Galicia, Avenida de Vigo s/n, E-15705 Santiago de Compostela, Spain*

³*Theoretical Division, Los Alamos National Laboratory, Los Alamos, New Mexico 87545, USA*

⁴*Department of Physics and Astronomy, University of Wyoming, Laramie, Wyoming 82071, USA*

⁵*Laboratoire de Physique des Solides, CNRS-UMR8502, Université de Paris-Sud, Orsay 91405, France*

⁶*Departamento de Física, FCEN, Universidad de Buenos Aires, Ciudad Universitaria Pabellón I, Buenos Aires 1428, Argentina*

⁷*Materials Science and Technology Division, Oak Ridge National Laboratory, Oak Ridge, TN 37831 and Department of Physics, University of Tennessee, Knoxville, TN 37996, USA*

We calculate the non-equilibrium electronic transport properties of a one-dimensional interacting chain at half filling, coupled to non-interacting leads. The interacting chain is initially in a Mott insulator state that is driven out of equilibrium by applying a strong bias voltage between the leads. For bias voltages above a certain threshold we observe the breakdown of the Mott insulator state and the establishment of a steady-state electronic current through the system. Based on extensive time-dependent density matrix renormalization group simulations, we show that this steady-state current always has the same functional dependence on voltage, independent of the microscopic details of the model and we relate the value of the threshold to the Lieb-Wu gap. We frame our results in terms of the Landau-Zener dielectric breakdown picture. Finally, we also discuss the real-time evolution of the current, and characterize the current-carrying state resulting from the breakdown of the Mott insulator by computing the double occupancy, the spin structure factor, and the entanglement entropy.

I. INTRODUCTION

The theoretical understanding of the non-equilibrium transport properties of strongly interacting systems in low dimensions has become a very active field of research, mainly due to the experimental activity in the fields of nanoscale materials^{1–3} and cold atomic gases,⁴ as well as due to advances in theoretical methods designed to deal with both the non-equilibrium situation *and* electronic correlations (see Refs. 5–7 for an overview and references therein). When considering non-equilibrium electronic transport, we have in mind a nanostructure that is subject to a large external voltage such that linear response theory does not apply anymore. The main theoretical question that one would like to address is the dependence of the electrical current on the applied voltage, i.e., the current-voltage characteristics, understanding not only the steady-state current reached on large time-scales, but also the transient regime appearing on shorter time-scales. Another important question is the characterization of the current-carrying state, contrasting its properties against equilibrium states in the absence of a voltage. From the experimental point of view, knowledge of the full dependence of the electronic current on the bias voltage through an interacting nanostructure is a question of utmost importance, as this measurement is a standard technique to map out electronic energy levels and to observe many-body effects in nanostructures (see, e.g., Ref. 8 for experimental work and Ref. 9 on theoretical work).

A paramount issue when studying transport in

strongly interacting systems is the behavior of the insulating states characteristic of these systems, the most relevant of which is the Mott insulator (MI) state. Considerable theoretical efforts have so far been devoted to the study of non-equilibrium transport in nanostructures such as quantum dots (see, e.g., Refs. 10–21). Using state-of-the-art-numerical approaches, substantial progress has been made in calculating the current-voltage characteristics and non-equilibrium properties of some basic models, such as the interacting resonant level model¹¹ or the single-impurity Anderson model^{10,14,16,17,21} as well as in understanding their transient behavior.^{14,22,23} Whereas quantum dots with an odd number of electrons exhibit perfect conductance in the low bias regime due to the Kondo effect,²⁴ an extended region with repulsive interactions, an even number of electrons, and at half filling is an insulator. The crossover from single quantum dots to this Mott insulating state has been studied in Refs. 25–27 on the level of linear response theory, showing that the ground state alternates between a conducting state for an odd number of sites and an insulating state for an even number of sites. Of course, in the limit of large systems, the difference between N and $N + 1$ electrons becomes irrelevant and the perfect conductance in a system with an odd number of electrons can only be observed at, with respect to experiments, unrealistically low energy scales.

In this paper, we shall thus turn our attention to non-equilibrium electronic transport through an extended interacting region, described by the one-dimensional Hubbard model with repulsive onsite interactions. Specifically we consider a one-dimensional (1D) system consist-

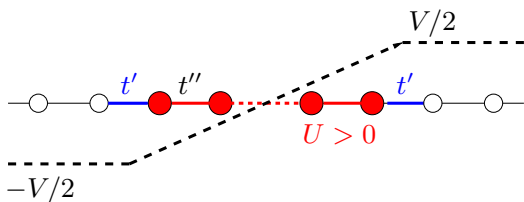


FIG. 1: (Color online) Sketch of the one-dimensional nanosystem described in the text, with an extended interacting region connected to non-interacting leads. Open (solid) symbols represent non-interacting (interacting) sites. The dashed line shows the voltage profile used to drive the system out of equilibrium. The voltage is homogeneous in the leads, and interpolates linearly between those values in the interacting region.

ing of an interacting region of length L_{int} connected to two non-interacting leads (see Fig. 1). The interacting region is initially in the MI state and we focus on the strongly interacting regime with interaction strength on the order or larger than the bandwidth. The sudden application of a large external voltage drives the system out of equilibrium and causes a time-dependent electrical current to flow through the interacting region, destroying the MI state. Our goals are first, to calculate the nonlinear current-voltage (I-V) characteristics; second, to contribute to the characterization of the current-carrying state; and third, to study the time-dependence of the entanglement entropy in this set-up. We employ the adaptive time-dependent density-matrix renormalization group (tDMRG) method,^{28,29} which has been successfully used to compute the non-equilibrium dynamics of single quantum dots.^{11,14,23,30,31}

The problem of destroying a MI by subjecting it to a voltage or an electric field is currently attracting significant attention, both for the 1D^{32–38} and the 3D cases,³⁹ as well as in heterostructures.^{40,41} In the case of an extended interacting region, the voltage can be applied with different spatial profiles in theoretical simulations, giving rise to different physical mechanisms for destroying the MI state. In the set-up sketched in Fig. 1, we linearly interpolate between the voltages set in the leads across the interacting region. As we shall argue, this gives rise to a many-body Landau-Zener mechanism through which the MI breaks down. This picture has been advocated for in a series of studies by Oka and collaborators,^{32–34,37} who considered both a ring geometry pierced by a time-dependent flux³² and a MI subject to a linear potential without including a coupling to leads.³⁴ Both approaches model the application of an electric field. One of their main results is that the breakdown of a MI is governed by the same physical laws as the one of a band insulator, with the difference that the band gap needs to be replaced by the charge gap of the strongly-interacting MI.^{32,34}

Our setup is chosen to closely catch features of an actual transport experiment by including the leads. We shall provide a qualitative comparison of our results with

other cases recently addressed in the literature.^{34,37–39} Transport through extended interacting regions that are not necessarily in a MI state has been studied as well in Refs. 42–46, emphasizing as recurring themes the appearance of nonlinear current-voltage characteristics and negative differential conductances.

Our main result is the accurate numerical calculation of steady-state currents for the geometry of Fig. 1. We find that the current-voltage characteristics can be described by an expression of the form

$$J(V) = aV e^{-V_c/V}, \quad (1)$$

in agreement with Refs. 32–34,37, implying that at sufficiently large voltages, the system is driven to a conducting state with $J \propto V$. We show that $V_c \propto \Delta_c^2$, where Δ_c is the Mott gap. In addition, we analyze several quantities in the current-carrying state, with a particular focus on the double occupancy and spin correlations. While the current-carrying state still has a tendency towards antiferromagnetic correlations, this instability is strongly suppressed compared to the MI state. However, neither the spin-structure factor nor the double occupancy, which is a measure of the interaction energy stored in the interacting region, saturate in the time window that we can access numerically. This suggests that the interacting region still undergoes a reorganization of internal energy while the particle flow in and out of the interacting region is already constant. The crossover from the insulating regime to the conducting regime is also reflected in the time-dependence of the entanglement entropy. We further show that this quantity behaves similarly to the case of global quenches: in our set-up, which is relevant for transport, the entanglement entropy increases linearly in time in the conducting regime. Here, the increase of entanglement is due to real particles moving around, different from the situation encountered in quantum quenches with homogeneous particle densities, in which propagating collective excitations induce entanglement.^{47,48}

One-dimensional Mott insulators can be realized experimentally in several classes of materials. A promising class of materials that have been suggested to realize 1D MI are carbon nanotubes.^{49–54} A recent experiment on carbon-nanotube field-effect devices made from small-band-gap and nominally metallic carbon nanotubes has shown evidence for the realization of such a MI state.⁵⁵ Theoretical work^{49,54} indicates that carbon nanotubes can be modeled by the Hubbard model on a two-leg ladder geometry. Since in this effort we are interested in the generic behavior of a MI in the non-equilibrium regime, and since we also need to keep the numerical effort at a manageable level, we will consider only 1D chains, as opposed to ladders. Nevertheless our results may set the grounds for future studies on the appealing two-leg ladder geometry.

Besides realizations in nanostructures, the electronic properties of some quasi-one dimensional transition metal oxides are known to be well described by the one-dimensional Hubbard model. Most notably, Mott insu-

lator physics was found to be realized in SrCuO₂ and Sr₂CuO₃ and the specific question of the dielectric breakdown of the MI state was experimentally addressed by Taguchi *et al.* in Ref. 56. The actual physics of this experiment, however, may go beyond a simple Hubbard model description, as has been emphasized by Eckstein, Oka, and Werner.³⁹

An additional and related line of experimental research uses time-resolved photoelectron spectroscopy to drive systems with a gap into gapless phases (see, e.g., Ref. 57). This method allows one to discriminate Mott insulators from other insulating states.

The outline of the paper is the following. In section II we present the model and briefly describe our numerical approach. In section III we present our results for real-time currents, spin correlations, the double occupancy, and the entanglement entropy. Section IV contains a summary and we discuss our results, contrasting them against the recent literature.

II. MODEL AND METHODS

To study the non-equilibrium transport in a Mott insulator we consider a one-dimensional chain with L electronic sites. The chain is divided into three different regions: a non-interacting region at the left, representing a lead; an interacting region in the center, where the Mott insulator state is located; and another non-interacting region at the right, representing another lead (see Fig. 1). This setup allows us to include the effects of the leads, complementary to the approach taken in Ref. 34. The number of sites of the left (right) lead is L_l (L_r), and in the interacting region is L_{int} . The Hamiltonian of the whole system can be written as

$$H = H_{\text{int}} + H_{\text{int-leads}} + H_{\text{leads}}, \quad (2)$$

where

$$H_{\text{int}} = -t'' \sum_{\sigma, i=L_1+1}^{L_1-1+L_{\text{int}}} (c_{i\sigma}^\dagger c_{i+1\sigma} + h.c.) + \epsilon_0 \sum_{\sigma, i=L_1+1}^{L_1+L_{\text{int}}} n_{i\sigma} + U \sum_{i=L_1+1}^{L_1+L_{\text{int}}} n_{i\uparrow} n_{i\downarrow} \quad (3)$$

is the Hamiltonian of a Hubbard chain with onsite Coulomb repulsion $U > 0$. t'' is the hopping matrix element between the sites in the interacting region, and ϵ_0 is the chemical potential in the interacting region. The second term in the Hamiltonian is

$$H_{\text{int-leads}} = -t' \sum_{\sigma} (c_{L_1\sigma}^\dagger c_{L_1+1\sigma} + h.c.) + c_{L_{\text{int}}+L_1\sigma}^\dagger c_{L_{\text{int}}+L_1+1\sigma} + h.c.), \quad (4)$$

connecting the Hubbard chain to the leads with a hopping t' , resulting in a tunneling rate $\Gamma = 2t'^2$. The third term in the Hamiltonian is

$$H_{\text{leads}} = -t_{\text{leads}} \sum_{\sigma, i=1}^{L_1-1} (c_{i\sigma}^\dagger c_{i+1\sigma} + h.c.) - t_{\text{leads}} \sum_{\sigma, i=L_1+L_{\text{int}}+1}^{L-1} (c_{i\sigma}^\dagger c_{i+1\sigma} + h.c.), \quad (5)$$

where t_{leads} is the hopping matrix element in the leads. In most simulations, we set $t' = t''$ and we use $t_{\text{leads}} = 1$ as the unit of energy unless stated otherwise. In all the equations above $c_{i\sigma}^\dagger$ represents the creation operator for an electron at site i and spin projection $\sigma = \uparrow, \downarrow$, $n_{i\sigma} = c_{i\sigma}^\dagger c_{i\sigma}$, and $n_i = n_{i\uparrow} + n_{i\downarrow}$.

We are interested in the time evolution of the MI state in the interacting portion of the chain when it is driven out of equilibrium by a strong voltage bias applied between the leads. Therefore, we first need to find the ground state of the system when the interacting portion of the chain is at half-filling ($\epsilon_0 = -U/2$) and then solve the time-dependent Schrödinger equation for the perturbed system with this state as an initial condition. The former is accomplished by performing a ground-state DMRG⁵⁸⁻⁶⁰ calculation with $N = L$ particles. To perturb the system and to drive the chain out of equilibrium we add an extra term to the Hamiltonian Eq. (2), which has the effect of adding an electric potential at time $t = 0$:

$$H_{\text{bias}} = \Theta(t) \sum_{i=1}^L V_i n_i,$$

where $\Theta(t)$ is the Heaviside step function and

$$V_i = \begin{cases} -V/2 & i \leq L_l \\ -(i - L_c) E & \text{for } L_l < i \leq L_l + L_{\text{int}} \\ V/2 & i > L_l + L_{\text{int}} \end{cases}, \quad (6)$$

where $L_c = L_l + (L_{\text{int}} + 1)/2$. This mimics the effect of an electric field $E = V/(L_{\text{int}} + 1)$ acting in the interacting part of the chain, V being the bias voltage induced between the leads (see Fig. 1).

To solve the time-dependent Schrödinger equation we use the adaptive time-dependent DMRG technique^{28,29} with the methods introduced in Refs. 11,14,23,30,31,61 to simulate non-equilibrium transport. In some cases, we use systems with L_l odd and L_r even since we find that the finite-size effects in the currents are less severe for this configuration (compare with Refs. 23,61,62 for the case of few quantum dots).

The tDMRG simulations are carried out using a third order Trotter-Suzuki breakup with a time-step of $\delta t = 0.1/t_{\text{leads}}$ and under the constraint of a fixed, maximum discarded weight of $\delta\rho \sim 10^{-7}$. In practice, this implies that one starts the time-evolution with a relatively small

number of states ($m \geq 100$) which then grows fast. The maximum number of states during the time-evolution is $m = 1600$ states. Since the accuracy of the numerical results solely depends on these control parameters, i.e., the discarded weight and the time step, tDMRG can be considered a quasi-exact method, as the numerical error can be estimated by varying δt and $\delta \rho$.

In non-equilibrium, the entanglement encoded in the time-dependent wave function is not bounded by any area law as is the ground-state entanglement⁶³ and may indeed increase extensively as a function of time. Typically, in so-called global quenches (i.e., the instantaneous and homogeneous change of one parameter on all sites) one finds a linear increase of the entanglement entropy (the von-Neumann entropy) $S_{vN} \sim t$ with time (see, e.g., Ref. 47 for the case of conformally invariant systems). Since the number of states m used in a DMRG calculation scales as⁶⁰

$$m \propto e^{S_{vN}}, \quad (7)$$

reaching long time scales is an exponentially expensive computational task whenever $S_{vN} \sim t$. Understanding the time-dependence of S_{vN} itself in generic setups is thus an important objective to judge limitations and capabilities of tDMRG, besides the general and timely interest in its time-dependence in various kinds of quenches.^{47,48,64}

The fact that the number of states increases monotonically with time defines a maximum time for each simulation as the time at which the number of states needed to keep the discarded weight under a fixed value $\delta \rho$ exceeds the maximum of $m = 1600$. Then, for representative parameters, we perform several runs with different $\delta \rho$ to assess and assure the numerical quality of the data, which ultimately determines the maximum time t_{\max} at which the data for a given observable are still sufficiently reliable.

We define the symmetrized tunnel current as the average of the two local currents connecting the interacting region to the left and right leads:

$$j = \frac{it'}{2} \sum_{\sigma} (c_{L_1, \sigma}^{\dagger} c_{L_1+1, \sigma} - \text{h.c.} + c_{L_1+L_{\text{int}}, \sigma}^{\dagger} c_{L_1+L_{\text{int}}+1, \sigma} - \text{h.c.}). \quad (8)$$

We will denote the time-dependent expectation value of the symmetrized current by $J(t) = \langle j(t) \rangle$ whereas the time-averaged current will simply be denoted as J . The currents are measured in units such that $J/V = 2$ corresponds to perfect conductance, i.e., $G_0 = 2e^2/h$ ($e = h = 1$ in our work). Local currents $\langle j_i \rangle$ on other bonds are defined accordingly.

III. RESULTS

The structure of this section is the following. First, we present the real-time data for the electric current and discuss the properties of the steady-state currents established after the dielectric breakdown of the Mott insulator takes place. Second, we analyze the current-voltage characteristics. As the main result of the paper we find a simple function to describe the current as a function of the bias voltage and the value of the Lieb-Wu gap associated to the initial Mott insulating state, similar to the results reported by Oka et al.^{34,37} Third, we characterize the current-carrying state in the interacting region by studying the time evolution of the charge and the current profiles, the double occupancy, and the spin-spin correlations. Finally, we discuss the time-dependence of the entanglement entropy.

A. Real-time data and steady-state currents

Figure 2 shows some examples of the real-time data for the symmetrized tunnel current obtained from our simulations for $U/t'' = 5$ and two values of Γ . The transient behavior, in general, can be expected to depend on both the tunneling rate, set by $\Gamma = 2(t'')^2$, and the voltage. For a small interacting region coupled to non-interacting leads, the transient regime has been studied in Refs. 14,22,23,65–67.

In our results, for all voltages, the generic behavior is that the current first goes through a transient regime, with a maximum reached in the time window $0 \leq t \leq 1/\Gamma$. The figure shows that the time-scale for reaching the first maximum is independent of the bias, while it clearly depends on Γ (this is obvious if one plots the results versus time in units of $1/t_{\text{leads}}$). Then, accompanied with oscillations whose period decreases with increasing voltage V , we reach a quasi-steady state regime (typically at times $t\Gamma \gtrsim 2 \dots 6$) where the current is constant, apart from oscillations. The amplitude of the oscillations decays as the steady-state is approached, yet from our data we cannot determine whether this decay is an exponential one or not. The period t_o of the oscillations is a monotonically decreasing function, similar to the case of single quantum dots in which $t_o \propto 1/V$.^{65,66}

The time window over which the steady-state current can be sustained on a finite system can in principle depend on both L and L_{int} . L trivially limits the accessible time-scales to $t < t_{\text{rec}} = 2(L - L_{\text{int}})/v_F$, where v_F is the Fermi velocity in the leads,^{14,23,61} since by that time, the perturbations induced in the leads by the application of the bias have traveled from the interacting region to the boundary and back, then perturbing the quasi-steady-state currents. L_{int} does not pose any limit on the stability of the steady-state regime for the setup considered here, because the bias voltage is introduced *locally* as a homogeneous electric field. Therefore we choose the values of L and L_{int} to give a value of t_{rec} similar to the

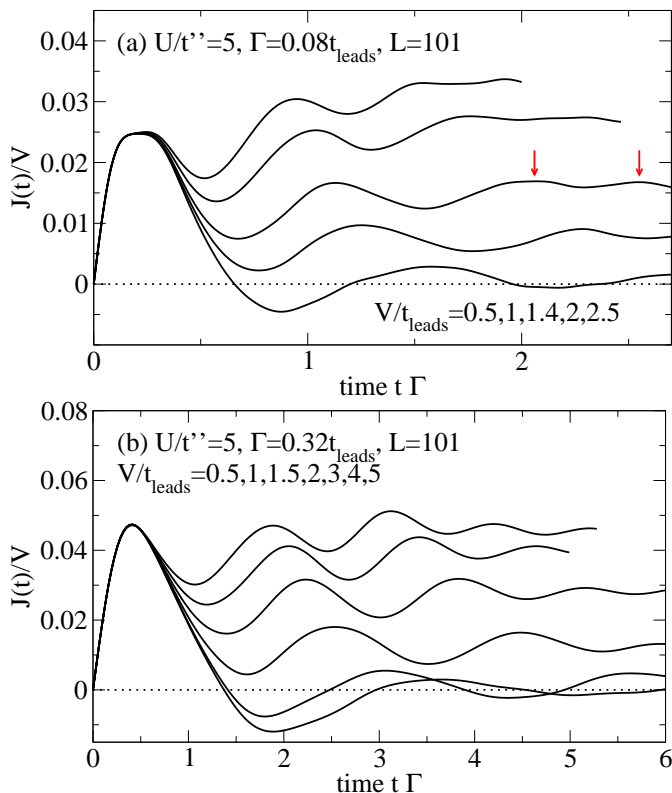


FIG. 2: (Color online) Current $J(t)$ as a function of time for $L_{\text{int}} = 20$, $U/t'' = 5$, $t' = t''$, $L = 101$ and (a) $\Gamma = 0.08t_{\text{leads}}$ (i.e. $t' = 0.2t_{\text{leads}}$), (b) $\Gamma = 0.32t_{\text{leads}}$ (i.e. $t' = 0.4t_{\text{leads}}$). In (a), $V/t_{\text{leads}} = 0.5, 1, 1.4, 2, 2.5$ (bottom to top) and in (b), $V/t_{\text{leads}} = 0.5, 1, 1.5, 2, 3, 4, 5$ (bottom to top). Note that the maximum time reached in these simulations are (a) $t = 40/t_{\text{leads}}$ and (b) $t = 20/t_{\text{leads}}$, in units of the inverse hopping matrix elements in the leads. The arrows in (a) indicate the time interval used to compute the steady-state current J for $V = 1.4t_{\text{leads}}$.

t_{max} discussed in the previous section, $t_{\text{rec}} \approx t_{\text{max}}$.

B. I-V characteristics

In this section we focus on the steady-state current and its dependence on the various parameters of the model, presenting results obtained from extensive numerical calculations. In practice, we compute the steady-state current by averaging over one or two periods of the oscillations at the longest times reached in the simulations (but $t < t_{\text{rec}}$) to reduce the effect of the oscillations. An example is shown with arrows in Fig. 2(a) for $V = 1.4t_{\text{leads}}$. We shall find that the current is a simple function of the bias voltage with all the microscopic details of the model encoded in the two coefficients a and V_c in Eq. (1). I-V curves were previously presented for the ring geometry for very short chains and in that case, the currents were extracted from the short-time dynamics.³²

Figure 3 shows the steady-state current J as a func-

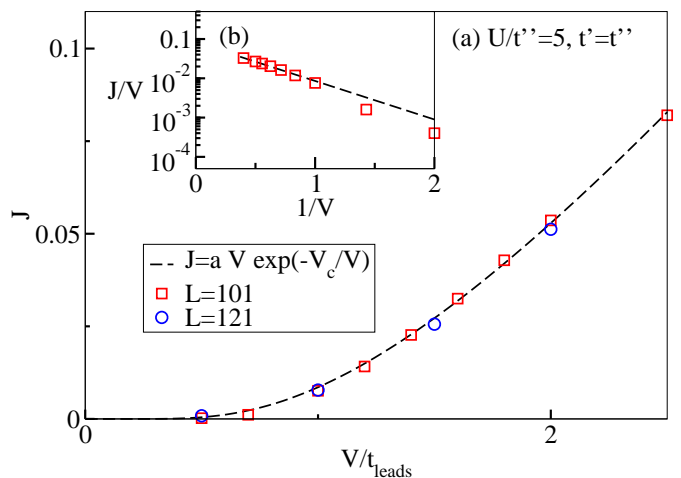


FIG. 3: (Color online) Current-voltage characteristics of the MI. Symbols represent the tDMRG results for the steady-state current, computed from the data shown in Fig. 2(a) as explained in Sec. III A. Dashed curves are fits to the function $J(V) = aV e^{-V_c/V}$, a and V_c being free parameters in the fit. (a) results for $U/t'' = 5$ with $t' = t'' = 0.2t_{\text{leads}}$. The plot includes data from two different system sizes to demonstrate that finite-size effects are small. (b) The inset shows the same data on a log-linear scale for $L = 101$. The agreement with the fit to Eq. (1) is excellent (except for very low bias voltages, where J is of the order of our numerical accuracy).

tion of the bias voltage V for $L_{\text{int}} = 20$ and $U/t'' = 5$ with $t' = t'' = 0.2t_{\text{leads}}$. The data from our numerical simulations for J as a function of the bias voltage fit to Eq. (1) with an excellent agreement, a and V_c being the fitting parameters. Therefore, for values of $V < V_c$ below the threshold V_c , J is exponentially suppressed whereas for values of $V > V_c$ above the threshold, J increases linearly. The exponential term is dominant at low bias and causes the suppression of the current and represents the Landau-Zener tunneling rate⁶⁸ across the Mott gap. The linear term is dominant at large bias and represents the motion of current-carrying excitations across the chain in the conducting regime.

Figure 4 contains the I-V curves for several different U/t'' , keeping t' and t'' fixed. Motivated by Fig. 2 from Ref. 32, we have plotted the steady-state current as a function of V/Δ_c^2 , where Δ_c is the charge gap. We have calculated the charge gap for finite systems with $L_{\text{int}} = 20$ sites, not connected to any leads, using

$$\Delta_c = [E_0(N+2, S^z) + E_0(N-2, S^z) - 2E_0(N, S^z)]/2, \quad (9)$$

where $E_0(N, S^z)$ is the ground state energy in subspaces with N fermions and a total spin projection S^z . Using this, and by also plotting the current in units of U^2 , all curves collapse on a single one, which, in particular, suggests $V_c \propto \Delta_c^2$, as expected for a Landau-Zener type of breakdown of the MI state.^{32,34} As we show here, this important fingerprint of Landau-Zener physics also survives upon coupling the interacting region to leads.

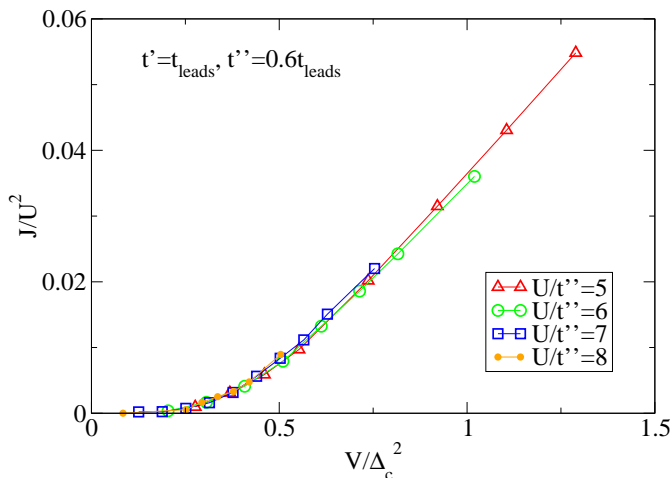


FIG. 4: (Color online) I-V curves for several U/t'' at fixed values of $t' = t_{\text{leads}}$ and $t'' = 0.6t_{\text{leads}}$. Δ_c is the charge gap computed for an isolated chain of $L_{\text{int}} = 20$ from Eq. (9). Symbols are tDMRG data for $L = 100$ ($L = 80$ for $U/t'' = 7$). Lines are guides to the eyes.

We here therefore find essentially the same dependence of V_c on U as Oka et al.,^{32,34} namely $V_c \propto \Delta_c^2$, but with incorporating the leads into the model. There are some differences, though. First, it should be noted that our time-averaged current is extracted from simulations that reach much longer times than Ref. 32 where only the short-time dynamics was available to estimate the steady-state currents. Second, we do not find an abrupt increase of the current at the threshold voltage, in contrast to Ref. 32. Therefore, our data are in a better agreement with the result of mapping the problem to a quantum walk (see Fig. 3 in Ref. 69). We attribute the quantitative differences between Fig. 5 in Ref. 32 and our Fig. 3 to the difference in the calculation of J , the fact that our systems are larger, and the inclusion of the leads.

To further explore the effect of the leads on V_c we have computed I-V curves for a fixed value of $U/t'' = 5$ and several t' , as shown in Fig. 5. Qualitatively, a larger t' leads to an overall increase of the current as reflected in the t' -dependence of a to be discussed later on. The threshold exhibits a weak dependence on t' as well, as we demonstrate in Fig. 6(a). Our observation is that $V_c(t' < t'') > V_c(t' = t'')$ and $V_c(t' > t'') < V_c(t' = t'')$. The latter behavior can be explained by the observation that close to the interface, the local charge gap depends on t' : $t' < t''$ leads to a slightly enhanced gap compared to the bulk gap and vice versa. As a consequence, the double occupancy $\langle d_i \rangle = \langle n_{i\uparrow} n_{i\downarrow} \rangle$ (discussed in detail below) in the interacting region is enhanced close to the interface compared to the bulk value for $t' > t''$, while it is suppressed for $t' < t''$. Therefore, for $t' < t''$ the contacts suppress the current, giving rise to an increase of V_c . In the case of $t' > t''$, the largest local gap is in the bulk of the MI and decreases towards the boundary.

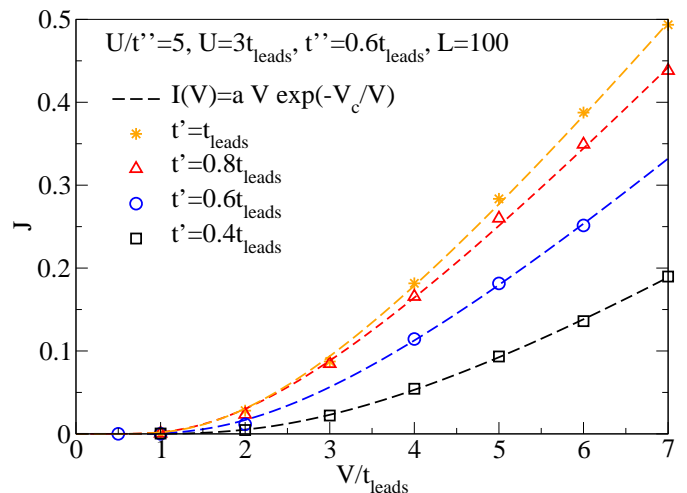


FIG. 5: (Color online) I-V curves for $t' \neq t''$ at a fixed $U/t'' = 5$ with $t'' = 0.6t_{\text{leads}}$. $t'/t_{\text{leads}} = 0.4, 0.6, 0.8, 1$ (bottom to top). Dashed curves are fits to the function $J(V) = aV e^{-V_c/V}$, with a and V_c being free parameters in the fit.

The decrease of V_c as $t' \rightarrow t_{\text{leads}}$ can be understood as a consequence of a smaller mismatch between t', t'' and t_{leads} in that limit, which should give rise to an increase in the transmission of electrons across the interface region. Note that we observe that boundary effects in the initial state typically decay to the bulk values over a distance of about 5 sites, suggesting that $L_{\text{int}} = 20$ is a reasonable choice to probe both the bulk and contact properties.

Next, we address the dependence of the prefactor a on t' . The coefficient a sets the value of the differential conductance in the conducting regime. We present our results for a and various combinations of t' in Fig. 6(b), in units of $G_0 = 2e^2/h$. Interestingly, in all cases studied, $a < 2G_0$. Moreover, this coefficient a monotonically increases with t' or $\Gamma = 2t'^2$. To summarize, a depends on both t' and U and, phenomenologically, we find that $a \propto U^2$ results in a convincing collapse of the I-V curves for $U > 4t''$ (compare Fig. 4).

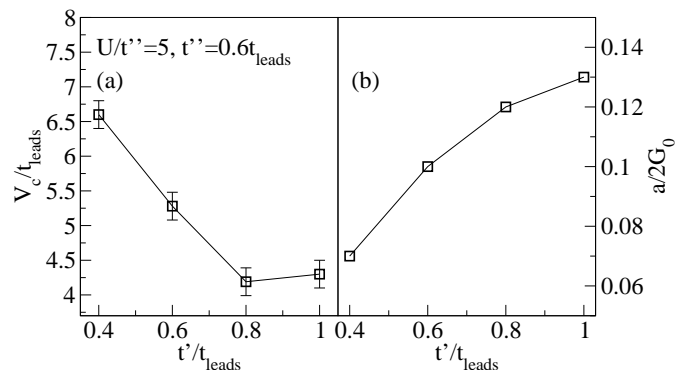


FIG. 6: (Color online) (a) Threshold voltage V_c vs. t' ; (b) prefactor a in Eq. (1) vs. t' . $U/t'' = 5$, $t'' = 0.6t_{\text{leads}}$, $L = 100$.

We have also studied the dependence of the I-V curves on L_{int} (not shown in the figures). We find that

$$V_c \propto (L_{\text{int}} + 1)\Delta_c^2 \quad \text{and} \quad a \sim 1/(L_{\text{int}} + 1). \quad (10)$$

This suggests that the breakdown should be viewed as *field-driven* with $E = V/(L_{\text{int}} + 1)$ taking the role of the electric field. We may therefore rewrite Eq. (1) as:

$$J = \tilde{a}E \exp(-E_c/E). \quad (11)$$

This interpretation is in agreement with Refs. 32,34,39, and we stress that the functional form of the I-V curve described by Eq. (11) holds despite the presence of the leads. As we have shown here, the effect of the leads is a small deviation of \tilde{a} and the threshold field E_c from the bulk values (compare Fig. 6 and Refs. 32,34).

C. Characterization of the current-carrying state

The goal of this section is to characterize the current-carrying state in the interacting region. To this end, we measure the electronic density and electronic current density profiles in the interacting region, the average double occupancy, and also the spin-spin correlations, yielding the spin structure factor.

1. Density and current profiles

Figure 7(a)-(c) show the charge density $\langle n_i \rangle$ as a function of position at different times for $U/t'' = 5$, $V = 2t_{\text{leads}}$, and $L_{\text{int}} = 20$ and the corresponding local currents $\langle j_i \rangle$ in (d)-(f). In the steady state, the charge in the interacting portion of the chain has a linear profile following the profile of the applied bias. The overall charge density in the Hubbard chain remains at half-filling.

From the results for the local currents, we see that the currents take finite values on all sites, which actually happens immediately after applying the potential. This clearly distinguishes the breakdown mechanism induced by a linear profile from other spatial forms of the bias voltage. For instance, in the simplest case in which $V_i = 0$ in the interacting region and $V_i = \pm V/2$ in the left(right) lead, the physics underlying the breakdown is quite different as we have verified in additional simulations (results not shown here). In this case, the redistribution of the charge inside the interacting region can be described as an effective doping of the MI region from the two interfaces. This implies that the bulk of the interacting region will experience the effects caused by turning on bias with a delay, set by the length of the interacting region.

Turning back to Fig. 7, to justify that the steady state in an extended system has been reached, the currents need to be constant both in time and space. From Fig. 7, we see that $\langle j_i \rangle = \text{const}$ is not fulfilled, although the

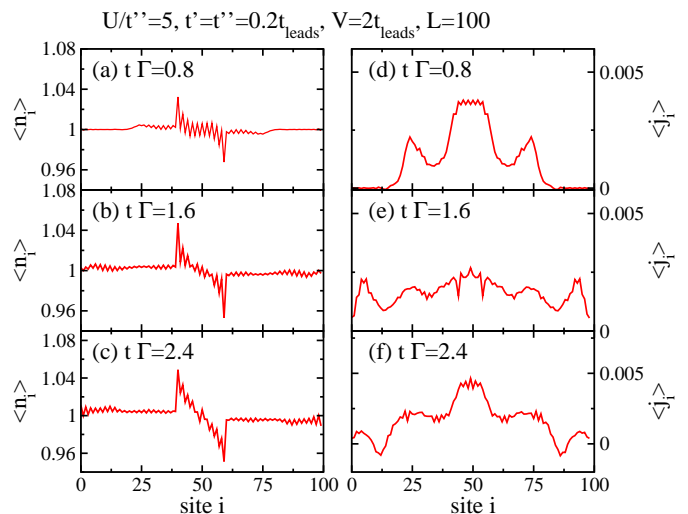


FIG. 7: (Color online) (a)-(c) Charge density $\langle n_i \rangle$ as a function of position at different times $t\Gamma = 0.8, 1.6, 2.4$ for $U/t'' = 5$, $t' = t'' = 0.2t_{\text{leads}}$, $V = 2t_{\text{leads}}$, and $L = 100$. (d)-(f) Profile of the local currents $\langle j_i \rangle$ at the same times as in panels (a)-(c).

charge flow in and out of the system is constant, apart from the relatively small oscillations discussed before (compare Fig. 2). This suggests that for the time scales reached in our simulations, the interacting region still undergoes a reorganization of charges and local energies. Indeed, from the data of Fig. 7, we find $\langle j_i - j_{i-1} \rangle \neq 0$, even at $t\Gamma \sim 2.5$.

2. Double occupancy

Figure 8 shows the average double occupancy per site in the interacting portion of the chain

$$d_{\text{av}}(t) = \frac{1}{L_{\text{int}}} \sum_{i=L_i+1}^{L_L+L_{\text{int}}} \langle d_i(t) \rangle \quad (12)$$

as a function of time for $U/t'' = 5$ and $V/t_{\text{leads}} = 0.5, 1, 1.4, 2$. At all these voltages, the average double occupancy oscillates with a period given by $t_o = t_o(V)$ that decreases with increasing voltage $1/V$, similar to the behavior of the currents.

Depending on the bias voltage two different behaviors can be observed. For bias voltages below the threshold $V < V_c$, i.e., in the regime of exponentially suppressed currents, $d_{\text{av}}(t)$ is essentially constant, apart from the oscillations. For bias voltages above the threshold $V > V_c$, $d_{\text{av}}(t)$ increases according to

$$d_{\text{av}}(t) = A + Bt + C \cos(Dt), \quad (13)$$

i.e., linearly in time after averaging over the period $t_o = 2\pi/D$. The slope B can be interpreted as the rate of the production of pairs of doublons and vacancies induced by the effective electric field.^{34,37} Quite notably,

the double occupancy never saturates over the time window simulated, i.e., a steady-state regime for this quantity is not reached in our simulations, even if the system is in the steady-state regime for the tunneling current. A similar observation has been made in the DMFT study by Eckstein *et al.*,³⁹ who also report a monotonically increasing double occupancy $d_{\text{av}}(t)$ in the steady-current regime. They ascribe this to the fact that the work done by the field is proportional to jE , which in a regime of constant currents is a constant. Hence this increase in energy has to go into the internal energy of the MI, in the absence of any dissipation or leads.

We shall here elaborate in more detail on this reasoning, adopting it to our set-up that includes the leads. To explain the time-dependence of d_{av} of Eq. (13) we exploit the fact that the equation of motion for the *average* double occupancy operator $\hat{d}_{\text{av}} = (1/L_{\text{int}}) \sum_{i=L_l+1}^{L_l+L_{\text{int}}} n_{i\uparrow} n_{i\downarrow}$ is the same as the one for the interaction energy. After some straightforward algebra, one gets

$$\frac{d}{dt} \hat{d}_{\text{av}} = \frac{1}{UL_{\text{int}}} \left(-\frac{d\hat{T}}{dt} + E \sum_{i=L_l+1}^{L_l+L_{\text{int}}-1} j_i \right), \quad (14)$$

where $\hat{T} = \hat{T}_{\text{int}} + \hat{T}_{\text{int-leads}}$ is the kinetic energy operator involving sites at the interacting region, and E is the constant electric field. For times in the steady-current regime, the time integration of the second term in the RHS gives a linear dependence on time, as the current is approximately constant. Assuming that d_{av} is small, as Fig. 7 suggests, we can expand the quantum mechanical average of the kinetic energy operator in the interacting region as $\langle \hat{T}_{\text{int}} \rangle \approx T_0 + \epsilon_d d_{\text{av}} + \mathcal{O}(d_{\text{av}}^2)$, where T_0 is the kinetic energy of the filled lower Hubbard band, and ϵ_d is the kinetic energy of a doublon. As a filled band cannot increase its kinetic energy, the time derivative approximates as $d\langle \hat{T}_{\text{int}} \rangle / dt \approx \epsilon_d dd_{\text{av}} / dt$. With this assumption one can move the contribution from \hat{T}_{int} to the LHS of Eq. (14) and conclude that the time derivative of the average double occupancy is

$$\frac{d}{dt} d_{\text{av}}(t) \propto -\frac{d}{dt} T_{\text{int-leads}} + E \sum_{i=L_l+1}^{L_l+L_{\text{int}}-1} j_i + \mathcal{O}(d_{\text{av}}(t)^2) \quad (15)$$

where all operators have been substituted by their quantum mechanical averages, and we have changed the equality in Eq. (15) to a proportionality to accommodate the term stemming from the kinetic energy of the doublons. The first term in the RHS is the energy flowing out of the interacting region carried away by the particles transferred to the leads. If the interacting part is an isolated system as in Ref. 39, this term is absent. The interpretation of Eq. (15) is that although the establishment of the steady-current regime implies a linear increase of the double occupancy and therefore of the interaction energy, part of this energy is transferred to the leads when accelerated particles leave the interacting region. This reduces the rate at which the double occupancy increases, allowing the system to stay in the steady-current regime for a

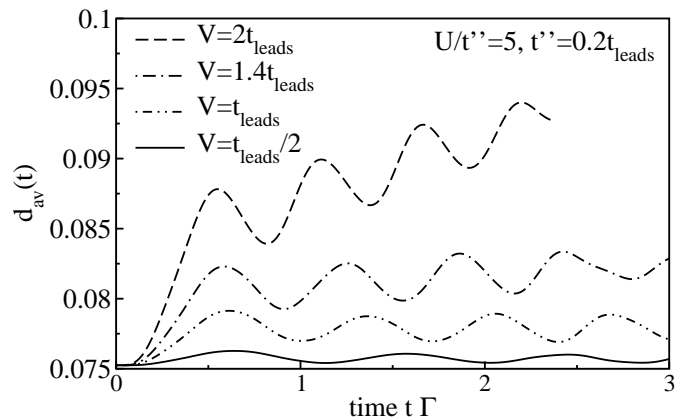


FIG. 8: (Color online) Average double occupancy $d_{\text{av}}(t)$ in the interacting region as a function of time for $U/t'' = 5$, $V/t_{\text{leads}} = 0.5, 1, 1.4, 2$, and $t' = t'' = 0.2t_{\text{leads}}$.

longer time. The increase in the double occupancy implies that the system is not in a true steady-state in the sense that there are observables that depend on time.

As for the existence and the nature of a true steady-state, two scenarios are conceivable. Obviously, due to the bounded spectrum, the increase of the double occupancy cannot go on forever, so eventually it has to saturate. An extreme case would be that d_{av} takes its maximum value $d_{\text{max}} = 0.5$ compatible with the system being at half filling on average. Consequently, the current would vanish in this case. Alternatively, the internal energy could saturate at some time, reflected in $d_{\text{av}} = \text{const} < 0.5$ (where the RHS is the maximum possible value assuming an average half filling of the interacting region). In that case, a finite current flow would be possible and the energy gain due to particles getting accelerated by the electric field would have to be balanced by an equal energy flow into the leads. In either case, the reorganization of doublons may take longer than the time needed to reach the steady-state regime for the current. In particular, it is well known that the dynamics of doublons in one-dimensional systems with $U > W$ where W is the bandwidth can be slow, if not even delayed by metastable regimes (see, e.g., Refs. 70–72 for 1D systems and Refs. 73 for higher dimensions). This aspect has also been touched upon in Ref. 39.

Unfortunately, our simulations are restricted in the accessible times, and we can thus not clarify this point, leaving it as an open question for future research.

3. Spin-spin correlations

The (longitudinal) spin structure factor can be computed from the spin-spin correlations by taking a Fourier transform ($i, j \in [L_l + 1, L_l + L_{\text{int}}]$):

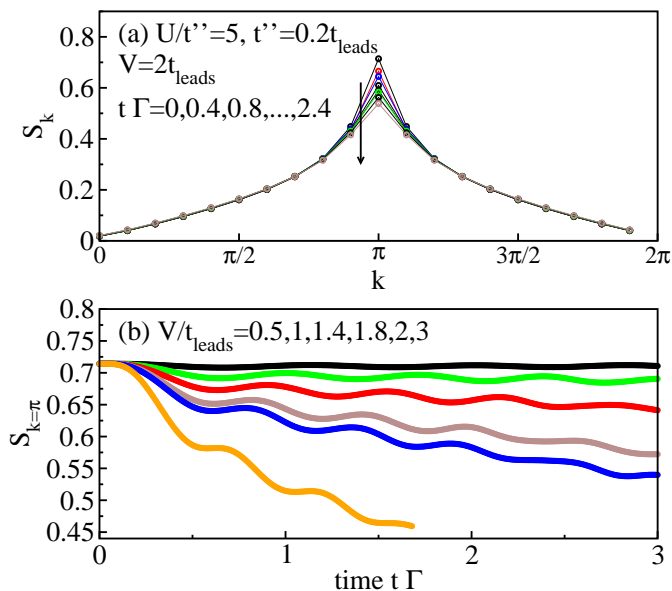


FIG. 9: (Color online) (a) Spin structure-factor in the interacting region as a function of time for $U/t'' = 5$ ($t' = t'' = 0.2t_{\text{leads}}$) and $V = 2t_{\text{leads}}$. (b) $S_{k=\pi}$ in the interacting region as a function of time for $V/t_{\text{leads}} = 0.5, 1, 1.4, 1.8, 2, 3$ (top to bottom).

$$S_k = \frac{1}{L_{\text{int}}} \sum_{l,m} e^{-i(l-m)k} \langle S_l^z S_m^z \rangle. \quad (16)$$

Figure 9(a) shows the spin structure-factor at different times for $U/t'' = 5.0$ and $V = 2t_{\text{leads}}$. The main feature is the survival of antiferromagnetic correlations in the current-carrying state: the shape of the spin structure-factor remains qualitatively the same, yet the weight of the $k = \pi$ instability decreases steadily with time. We therefore show $S_{k=\pi}(t)$ for several bias values V in Fig. 9(b) as a function of time. The figure unveils that, similar to the case of the average double occupancy, a steady-state regime for this observable is not reached in our simulations, i.e., on the longest times reached and for the system sizes considered here. Similar to the linear *increase* of the average double occupancy, the $S_{k=\pi}(t)$ *decreases* linearly in time.

D. Entanglement entropy

The entanglement entropy is defined as

$$S_{vN,x} = -\text{tr}[\rho_x \ln(\rho_x)], \quad (17)$$

where ρ_x is the reduced density matrix of a block of the length x (counting from the left end of the chain). The reduced density matrix and its spectrum of eigenvalues is a key object in DMRG and the entanglement entropy is thus one of the easiest accessible quantities.⁶⁰

Let us begin by recalling some established analytical results on the entanglement growth in quantum quenches in systems with conformal invariance: In a *global* quench (i.e., the change of a parameter on all sites), $S_{vN,x} \propto t$ (Ref. 47) whereas in a *local* quench, $S_{vN,x} \propto \ln(t/t_0)$.^{48,74} For the case of a global quench, this has been confirmed in numerous numerical calculations, mostly using DMRG (see, e.g., Refs. 75,76).

Our situation is different, since a parameter - the bias voltage - is changed on all sites, but with an explicit site dependence. Our results for $S_{vN,x} = S_{vN,x}(t)$ are displayed in Fig. 10. Panel (a) shows $S_{vN,x} = S_{vN,x}(t)$ vs. x for all possible cuts accessed in a DMRG run for a fixed value of $V = 2t_{\text{leads}}$ at different times. The overall increase of $S_{vN,x}$ as a function of time is evident.

The key question here is how the flow of particles in the conducting regime gives rise to an increased entanglement between, say, the left lead and the rest of the system. In particular, we expect basically no increase in the insulating regime of bias voltages $V < V_c \propto \Delta_c^2$. To address this point, we plot $S_{vN,x}(t)$ with $x = L_l$ in Fig. 10(b) for several bias voltages. Generally, we find that $S_{vN,x} = ct$. The dependence of the prefactor c on bias voltage V is shown in the inset of Fig. 10(b): its dependence on V can be described by the same functional form as the tunnel current, namely:

$$c \propto V \exp(-V_{c,vN}/V). \quad (18)$$

In particular, we find that $V_{c,vN} \approx V_c$ within the accuracy of our numerical simulations, where V_c is the threshold voltage extracted from Fig. 3. This is consistent with the picture that entanglement is predominantly induced by propagating particles, in contrast to global quenches, in which $\langle n_i(t) \rangle = \text{const}$.

While the observation of $S_{vN,x} \propto t$ implies that the simulations carried out here become exponentially costly at long times, we note that in similar set-ups, namely the case in which a confining potential of a linear form is present in the *initial* state and its removal at $t = 0$ is used to drive the time-evolution, a weaker logarithmic increase is found. Specifically, for the exactly solvable *XX* model, Eisler et al. report $S_{vN,x} \propto \ln(t)$.⁶⁴ Two main differences between their set-up and ours need to be pointed out. First, in our case, the application of the bias V_i destroys the MI state *and* drives the current flow. Conversely, in the set-up of Ref. 64, the initial state already has an inhomogeneous particle density, implying that correlations in the initial state are already very different from the respective ground state ones at the same filling. These open questions and observations call for a full analysis of the behavior of $S_{vN,x}$ in global quenches with site dependent changes of parameter, that we leave as a future project.

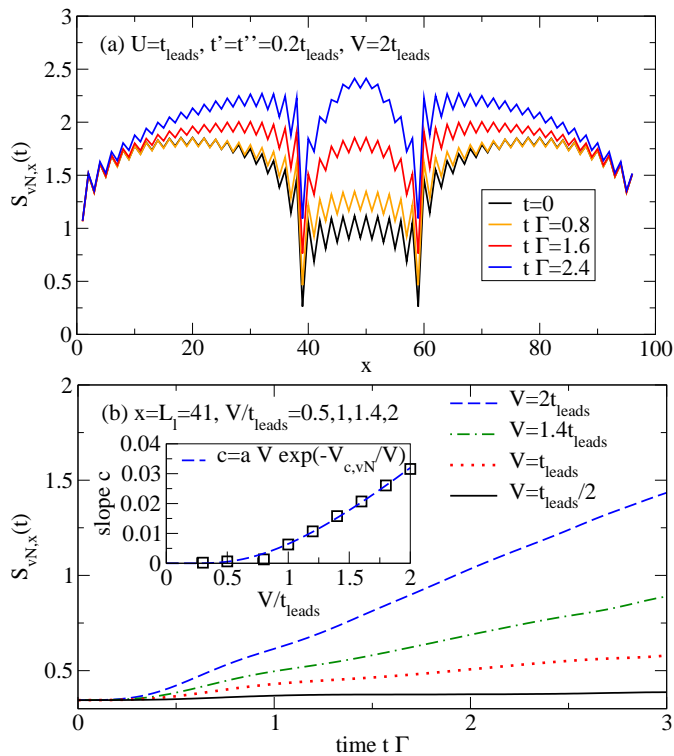


FIG. 10: (Color online) (a) Entanglement entropy $S_{vN,x}(t)$ vs. position x of the cut taken in the bipartition for times $t\Gamma = 0, 0.8, 1.6, 2.4$. (b) $S_{vN,x}(t)$ vs. time t for $x = L_l = 41$. This cuts the system across the left link that connects the left lead to the interaction region ($V/t_{\text{leads}} = 0.5, 1, 1.4, 2$, from bottom to top). Inset: slope c of $S_{vN,x}(t) = ct$ computed in the time-interval $t\Gamma \in [0.25, 3]$. The dashed line is a fit to $c = aV \exp(-V_{c,vN}/V)$. In both panels, $U/t'' = 5$, $t' = t'' = 0.2t_{\text{leads}}$.

IV. DISCUSSION

In this paper we have studied the dielectric breakdown of a Mott insulator state in a realistic model with an interacting chain connected to non-interacting leads. Our numerical results confirm that the steady-state current as a function of the applied voltage is, over a wide range of voltages, described by a simple universal function, with all the microscopic details of the model encoded in two coefficients related to the conductance in the metallic regime and the value of the threshold voltage. Our work further elucidates the influence of contacts to the leads on the I-V curve: the overall current is a monotonically increasing function in the inverse tunneling rate $1/\Gamma$ and the threshold, on finite systems, also exhibits a weak dependence on the contacts.

The dielectric breakdown of the one-dimensional Hubbard model was studied under dissipative tunnelling into the environment introduced by a imaginary gauge potential in Ref. [77], and upon the application of a strong electric field introduced by a gauge potential in a ring geometry in Refs. [32–34,37]. The main conclusion of

the latter papers is that the dielectric breakdown of the Mott insulator can be understood in the same terms as the one in band insulators, with the only change that the band gap has to be substituted for with the Mott gap in the calculation of the Landau-Zener parameter (i.e., the threshold field). The time-averaged current in small Hubbard rings shows a collapse of the currents to a universal curve when the currents are plotted as a function of the Landau-Zener parameter,³² sharing the same qualitative traits as our Fig. 3, with a negligible current before the breakdown and a linear I-V characteristics at biases larger than the threshold. An important conclusion of our work is the confirmation that the mechanism of the dielectric breakdown corresponds to the Landau-Zener tunneling mechanism and this mechanism survives upon coupling the interacting region to leads.

It should be noted that another very recent tDMRG study by Kirino and Ueda³⁸ has addressed the destruction of the MI state upon application of a strong voltage as well. There are important differences with our work, though. In Ref. 38, no leads are included, and the bias is applied as a step-function function to a homogeneous MI, measuring the local current on the central link. While the I-V curve also shows an activated behavior, it is not clear whether the MI is also destroyed through a Landau-Zener mechanism in the set-up of Kirino and Ueda. In particular, they report $V_c \propto \Delta_c$, in contrast to the results by Oka et al. and ours (compare Fig. 4). This illustrates the rich and various physical scenarios that can underlie the breakdown of an insulating state, depending on the way the bias is applied.

We have also studied the conducting state that is reached after the breakdown. The spin-spin correlations remain antiferromagnetic in the steady state. A decrease in the amplitude of the correlations is observed as the bias exceeds the threshold value. The conducting state can also be distinguished from the initial insulator by an increase in the double occupation. In other words, the electric field creates excitations as pairs of doublons and holons that can carry the current.⁷⁸ The production rate of these excitations should be reflected in the production rate of doubly occupied sites. Quite notably, the time-dependence of both the double occupancy and the spin-spin correlations implies that the interacting region is not in a true steady state yet, in which these quantities would become stationary as well.

Finally, we have also computed the time-dependence of the entanglement entropy. This quantity increases linearly with time in the conducting regime, implying that tDMRG simulations become exponentially expensive at long times. On the positive side, studying transport through single quantum dots or extended structures has qualitatively the same computational complexity, since in both cases, $S_{vN,x} \propto t$ (unpublished results for one quantum dot, see Ref. 14). Therefore, going from single to many quantum dots is equally feasible with this method, in contrast to other state-of-the-art techniques such as time-dependent NRG¹⁰ or real-time QMC.¹⁶ In

the former, the complexity scales with the dimension of the interacting region and in the latter approach, the dynamical sign-problem is expected to become more severe for structures more complex than a single quantum dot. We have here demonstrated that tDMRG can successfully be applied to compute I-V curves of extended systems, complementing our earlier work on non-equilibrium transport in the single-impurity problem.^{14,30,61}

While our numerical analysis of several properties of the current-carrying state should be helpful in better understanding its properties, we acknowledge that a more intuitive picture of the non-equilibrium steady-state is still desirable. For instance, one would like to contrast the current-carrying steady-state against effective ground-state reference systems, an approach which in certain non-equilibrium cases works quite well.⁷⁹ Moreover, the interesting concept of an effective temperature, often used in studies of quantum quenches with a relaxation into a thermalized state (see Ref. 80 and references therein), should be further explored for current-carrying states.

In conclusion, we have shown that the dielectric breakdown of the Mott insulator can be understood in terms of the Landau-Zener mechanism using a realistic setup that matches the experiment since we include the leads. Furthermore we have been able to fully characterize the steady-state currents as a function of the bias voltage with a simple form, covering the whole range of voltages and microscopic parameters, that can be experimentally tested.

Acknowledgments

We thank M. Daghofer, H. Onishi, G. Roux and D. Schuricht for very useful discussions. I.G. acknowledges support from MICINN through grant FIS2009-13520. A.E.F. thanks NSF for support through grant DMR-0955707. E.D. is supported by the Division of Materials Science and Engineering, Office of Basic Energy Sciences, U.S. Department of Energy.

-
- * Corresponding author: heidrich-meisner@lmu.de
- ¹ W. G. van der Wiel, S. D. Franceschi, T. Fujisawa, J. M. Elzerman, S. Tarucha, and L. P. Kouwenhoven, *Science* **289**, 2105 (2000).
 - ² M. Grobis, I. G. Rau, R. M. Potok, H. Shtrikman, and D. Goldhaber-Gordon, *Phys. Rev. Lett.* **100**, 246601 (2008).
 - ³ G. D. Scott, Z. K. Keane, J. W. Ciszek, J. M. Tour, and D. Natelson, *Phys. Rev. B* **79**, 165413 (2009).
 - ⁴ I. Bloch, J. Dalibard, and W. Zwerger, *Rev. Mod. Phys.* **80**, 885 (2008).
 - ⁵ J. Eckel, F. Heidrich-Meisner, S. Jakobs, M. Thorwart, M. Pletyukhov, and R. Egger, *New J. Phys.* **12**, 043042 (2010).
 - ⁶ S. Andergassen, V. Meden, H. Schoeller, J. Splettstoesser, and M. R. Wegewijs, *Nanotechnology* **21**, 272001 (2010).
 - ⁷ M. Eckstein, A. Hackl, S. Kehrein, M. Kollar, M. Moeckel, P. Werner, and F. A. Wolf, *Eur. Phys. J. Special Topics* **180**, 217 (2010).
 - ⁸ W. G. van der Wiel, S. De Franceschi, J. M. Elzerman, T. Fujisawa, S. Tarucha, and L. P. Kouwenhoven, *Rev. Mod. Phys.* **75**, 1 (2002).
 - ⁹ K. A. Al-Hassanieh, C. Büsser, and G. Martins, *Mod. Phys. Lett. B* **23**, 2193 (2009).
 - ¹⁰ F. B. Anders, *Phys. Rev. Lett.* **101**, 066804 (2008).
 - ¹¹ E. Boulat, H. Saleur, and P. Schmitteckert, *Phys. Rev. Lett.* **101**, 140601 (2008).
 - ¹² S. Weiss, J. Eckel, M. Thorwart, and R. Egger, *Phys. Rev. B* **77**, 195316 (2008).
 - ¹³ A. Feiguin, P. Fendley, M. P. Fisher, and C. Nayak, *Phys. Rev. Lett.* **101**, 236801 (2008).
 - ¹⁴ F. Heidrich-Meisner, A. Feiguin, and E. Dagotto, *Phys. Rev. B* **79**, 235336 (2009).
 - ¹⁵ E. Sela and I. Affleck, *Phys. Rev. Lett.* **102**, 047201 (2009).
 - ¹⁶ P. Werner, T. Oka, M. Eckstein, and A. J. Millis, *Phys. Rev. B* **81**, 035108 (2010).
 - ¹⁷ M. Schiró, *Phys. Rev. B* **81**, 085126 (2010).
 - ¹⁸ S. G. Jakobs, M. Pletyukhov, and H. Schoeller, *Phys. Rev. B* **81**, 195109 (2010).
 - ¹⁹ C. Karrasch, S. Andergassen, M. Pletyukhov, D. Schuricht, L. Borda, V. Meden, and H. Schoeller, *EPL* **90**, 30003 (2010).
 - ²⁰ S.-P. Chao and G. Palacios, *arXiv:1005.5395* (unpublished).
 - ²¹ L. Muehlbacher, D. Urban, and A. Komnik, *arXiv:1007.1793* (unpublished).
 - ²² T. L. Schmidt, P. Werner, L. Mühlbacher, and A. Komnik, *Phys. Rev. B* **78**, 235110 (2008).
 - ²³ A. Branschädel, G. Schneider, and P. Schmitteckert, *Ann. Phys. (Berlin)* **522**, 657 (2010).
 - ²⁴ A. Hewson, *The Kondo Problem to Heavy Fermions*, Cambridge, UK, 1993.
 - ²⁵ A. Oguri, *Phys. Rev. B* **56**, 13422 (1997).
 - ²⁶ A. Oguri, *Phys. Rev. B* **59**, 12240 (1999).
 - ²⁷ A. Oguri, *Phys. Rev. B* **63**, 115305 (2001).
 - ²⁸ S. R. White and A. E. Feiguin, *Phys. Rev. Lett.* **93**, 076401 (2004).
 - ²⁹ A. Daley, C. Kollath, U. Schollwöck, and G. Vidal, *J. Stat. Mech.: Theory Exp.*, P04005 (2004).
 - ³⁰ L. G. G. V. Dias da Silva, F. Heidrich-Meisner, A. E. Feiguin, C. A. Büsser, G. B. Martins, E. V. Anda, and E. Dagotto, *Phys. Rev. B* **78**, 195317 (2008).
 - ³¹ S. Kirino, T. Fujii, J. Zhao, and K. Ueda, *J. Phys. Soc. Jpn.* **77**, 084704 (2008).
 - ³² T. Oka, R. Arita, and H. Aoki, *Phys. Rev. Lett.* **91**, 066406 (2003).
 - ³³ T. Oka, R. Arita, and H. Aoki, *Physica B* **359-361C**, 759 (2005).
 - ³⁴ T. Oka and H. Aoki, *Phys. Rev. Lett.* **95**, 137601 (2005).
 - ³⁵ S. Dutta, S. Lakshmi, and S. Pati, *J. Phys. Condens. Matter* **19**, 322201 (2007).
 - ³⁶ S. Dutta and S. Pati, *J. Phys. Condens. Matter* **20**, 075226 (2008).
 - ³⁷ T. Oka and H. Aoki, *Phys. Rev. B* **81**, 033103 (2010).

- ³⁸ S. Kirino and K. Ueda, *J. Phys. Soc. Jpn.* **i79**, 093710 (2010).x.
- ³⁹ M. Eckstein, T. Oka, and P. Werner, *Phys. Rev. Lett.* **105**, 146404 (2010).
- ⁴⁰ S. Okamoto, *Phys. Rev. B* **76**, 035105 (2007).
- ⁴¹ S. Okamoto, *Phys. Rev. Lett.* **101**, 116807 (2008).
- ⁴² T. Prosen and M. Žnidarič, *J. Stat. Mech.: Theor. Exp.*, P02035 (2009).
- ⁴³ M. Michel, O. Hess, H. Wichterich, and J. Gemmer, *Phys. Rev. B* **77**, 104303 (2008).
- ⁴⁴ G. Benenti, G. Casati, T. Prosen, and D. Rossini, *Europhys. Lett.* **85**, 37001 (2009).
- ⁴⁵ G. Benenti, G. Casati, T. Prosen, D. Rossini, and M. Žnidarič, *Phys. Rev. B* **80**, 035110 (2009).
- ⁴⁶ M. Mierzejewski and P. Prelovšek, *Phys. Rev. Lett.*, in press, arXiv:1007.3383 (unpublished).
- ⁴⁷ P. Calabrese and J. J. Cardy, *J. Stat. Mech.: Theory Exp.*, P04010 (2005).
- ⁴⁸ P. Calabrese and J. Cardy, *J. Stat. Mech.: Theory Exp.*, P06008 (2007).
- ⁴⁹ L. Balents and M. P. A. Fisher, *Phys. Rev. B* **55**, R11973 (1997).
- ⁵⁰ Y. A. Krotov, D.-H. Lee, and S. G. Louie, *Phys. Rev. Lett.* **78**, 4245 (1997).
- ⁵¹ H.-H. Lin, *Phys. Rev. B* **58**, 4963 (1998).
- ⁵² A. A. Odintsov and H. Yoshioka, *Phys. Rev. B* **59**, R10457 (1999).
- ⁵³ A. A. Nersesyan and A. M. Tsvelik, *Phys. Rev. B* **68**, 235419 (2003).
- ⁵⁴ C. Kane, L. Balents, and M. P. A. Fisher, *Phys. Rev. Lett.* **79**, 5086 (1997).
- ⁵⁵ V. V. Deshpande, B. Chandra, R. Caldwell, D. Novikov, J. Hone, and M. Bockrath, *Science* **323**, 106 (2009).
- ⁵⁶ Y. Taguchi, T. Matsumoto, and Y. Tokura, *Phys. Rev. B* **62**, 7015 (2000).
- ⁵⁷ L. Perfetti, P. Loukakos, M. Lisowski, U. Bovensiepen, M. Wolf, H. Berger, S. Biermann, and A. G. 3, *New J. Phys.* **10**, 053019 (2008).
- ⁵⁸ S. R. White, *Phys. Rev. Lett.* **69**, 2863 (1992).
- ⁵⁹ S. R. White, *Phys. Rev. B* **48**, 10345 (1993).
- ⁶⁰ U. Schollwöck, *Rev. Mod. Phys.* **77**, 259 (2005).
- ⁶¹ K. A. Al-Hassanieh, A. E. Feiguin, J. A. Riera, C. A. Büsser, and E. Dagotto, *Phys. Rev. B* **73**, 195304 (2006).
- ⁶² F. Heidrich-Meisner, G. B. Martins, C. A. Büsser, K. A. Al-Hassanieh, A. E. Feiguin, G. Chiappe, E. V. Anda, and E. Dagotto, *Eur. Phys. J. B* **67**, 527 (2009).
- ⁶³ J. Eisert, M. Cramer, and M. B. Plenio, *Rev. Mod. Phys.* **82**, 277 (2010).
- ⁶⁴ V. Eisler and I. Peschel, *J. Stat. Mech.: Theor. Exp.*, P02011 (2009).
- ⁶⁵ A. Schiller and S. Hershfield, *Phys. Rev. B* **62**, R16271 (2000).
- ⁶⁶ M. Pletyukhov, D. Schuricht, and H. Schoeller, *Phys. Rev. Lett.* **104**, 106801 (2010).
- ⁶⁷ A.-P. Jauho, N. S. Wingreen, and Y. Meir, *Phys. Rev. B* **50**, 5528 (1994).
- ⁶⁸ C. Zener, *Proc R. Soc. London A* **137**, 696 (1932).
- ⁶⁹ T. Oka, N. Komno, R. Arita, and H. Aoki, *Phys. Rev. Lett.* **94**, 100602 (2005).
- ⁷⁰ K. A. Al-Hassanieh, F. A. Reboredo, A. E. Feiguin, I. González, and E. Dagotto, *Phys. Rev. Lett.* **100**, 166403 (2008).
- ⁷¹ F. Heidrich-Meisner, S. R. Manmana, M. Rigol, A. Muramatsu, A. E. Feiguin, and E. Dagotto, *Phys. Rev. A* **80**, 041603(R) (2009).
- ⁷² L. G. G. V. Dias da Silva, K. A. Al-Hassanieh, A. E. Feiguin, F. A. Reboredo, and E. Dagotto, *Phys. Rev. B* **81**, 125113 (2010).
- ⁷³ A. Rosch, D. Rasch, B. Binz, and M. Vojta, *Phys. Rev. Lett.* **101**, 265301 (2008).
- ⁷⁴ V. Eisler and I. Peschel, *J. Stat. Mech.: Theory Exp.*, P06005 (2007).
- ⁷⁵ A. Laeuchli and C. Kollath, *J. Stat. Mech.: Theory Exp.*, P05018 (2008).
- ⁷⁶ G. D. Chiara, S. Montangero, P. Calabrese, and R. Fazio, *J. Stat. Mech.: Theory Exp.*, P03001 (2006).
- ⁷⁷ T. Fukui and N. Kawakami, *Phys. Rev. B* **58**, 16051 (1998).
- ⁷⁸ Y. Kluger, J. M. Eisenberg, B. Svetitsky, F. Cooper, and E. Mottola, *Phys. Rev. Lett.* **67**, 2427 (1991).
- ⁷⁹ F. Heidrich-Meisner, M. Rigol, A. Muramatsu, A. E. Feiguin, and E. Dagotto, *Phys. Rev. A* **78**, 013620 (2008).
- ⁸⁰ M. Cazalilla and M. Rigol, *New J. Phys.* **12**, 055006 (2010).